Experimental verification of quantum contextuality using a weak measurement in a single trapped ion

Chunwang Wu [1,2] Han Hu,[1,2,3,*] Jie Zhang,[1,2] Wenbo Su,[1,2] Manchao Zhang,[1,2] Tianxiang Zhan [1,2] Qingqing Qin [1,2] Wei Wu,[1,2] and Pingxing Chen[1,2,†]

[1]*Institute for Quantum Science and Technology, College of Science, National University of Defense Technology, Changsha 410073, Hunan, China*

[2]*Hunan Key Laboratory of Quantum Information Mechanism and Technology, National University of Defense Technology, Changsha 410073, Hunan, China*

[3]*Northwest Institute of Nuclear Technology, Xi'an 710024, Shanxi, China*

Quantum contextuality is usually verified through establishing the violation of appropriate inequalities constructed based on the assumption of generalized noncontextuality. Recently, the connection between anomalous weak values (AWVs) and the generalized contextuality under specific experimental conditions has been proposed. Experimentally, only the connection between the real part of the AWVs and the generalized contextuality is verified in a single-photon experimental system. In this paper, we conduct weak measurement experiments in a single $^{40}Ca^+$ ion system under specific experimental conditions. The incompatibility between quantum mechanics and noncontextual ontological models (NCOMs) is verified by both the real and imaginary parts of the AWVs, which provides a more general test of the connection between the quantum contextuality and AWVs.

I. INTRODUCTION

Quantum contextuality refers to the fact that it is not possible to give a noncontextual classical interpretation of quantum predictions in terms of ontic states [1]. In 1967, the Kochen-Specker (K-S) theorem denied the noncontextual hidden-variable model of quantum theory using a set of 117 incompatible observables and established the notion of quantum contextuality [2]. Several attempts have been made to simplify Kochen and Specker's proof, especially to reduce the number of different quantum observables used [3–6]. Then, to circumvent the experimental difficulties of verifying multiple algebraic equations and measuring many observables in tests of the K-S theorem, various kinds of K-S inequalities with more experimental ease were proposed to verify quantum contextuality, e.g., the state-dependent Clifton inequality [7], the Klyachko-Can-Binicioğlu-Shumovsky (KCBS) inequality [8], and the state-independent Yu-Oh inequality [9]. Up to now, quantum contextuality has been tested in experiments with trapped ions [10–12], photons [13,14], molecular nuclear spins [15], nuclear spins [16], and superconducting systems [17].

In 2005, Spekkens generalized the conventional K-S notion of contextuality in the operational framework, and granted it a much more broadly applicable scope [18]. Compared with the K-S contextuality, which is applicable only to projective measurements, Spekkens' generalized contextuality can be applied to all operational procedures, including unsharp measurements, preparations, and transformations. Recently, it has been established that the generalized contextuality forms the basis of quantum advantage in various information processing tasks, e.g., universal quantum computation [19], state discrimination [20], state-dependent cloning [21], quantum random access codes [22], quantum weak measurement technique [23], and so on. Correspondingly, the noncontextual bounds that quantify how well any noncontextual theory can perform in these tasks constitute noncontextuality inequalities whose violation can be used to witness the generalized contextuality [20–23].

Here, we focus on the noncontextuality inequality derived from the quantum weak measurement scenario. Weak measurement, with its outcome referred to as weak value, is a new measurement method that amplifies signals by selecting appropriate pre and postselected states under the weak coupling [24]. Different from the strong measurement, a weak measurement has the characteristics of less disturbance and less information extraction [25]. Recent works have shown that the incompatibility of quantum theories with noncontextual ontological models (NCOMs) can be proven in the framework of anomalous weak values (AWVs) [26]. It has been theoretically proven that the AWV is a full proof of the generalized contextuality under certain extra operational facts [23], and then the connection between the real part of the AWV and the generalized contextuality has been verified in a single-photon experimental system [27]. In 2019, Kunjwal *et al.* theoretically proved that the nonzero imaginary part of the weak value, seen as a new class of AWVs, can be used to manifest the contradiction between the generalized contextuality and NCOMs with a more tightened inequality [28], however, which still lacks the experimental test.

---
*1617830020@qq.com

†pxchen@nudt.edu.cn

In this paper, we use the experimental techniques of atomic weak value amplification in Refs. [29,30] to verify the connection between both the real and imaginary parts of AWVs with the generalized contextuality. This experiment proves the relationship between the imaginary parts of AWVs and the generalized contextuality. Our results clearly violate the noncontextual bound for the NCOMs, which provides a good demonstration of the connection between AWVs and the intrinsic contextuality of quantum mechanics.

II. THEORETICAL MODEL

A. Anomalous weak values

The principle of weak measurement [24,25,29–33] can be explained by von Neumann's measurement model. According to the measurement process proposed by von Neumann [34], we use a pointer to couple with the measured system and the Hamiltonian describing the coupling interaction between the pointer and the measured system can be written as

$$H_I = g\hat{A} \otimes \hat{p}. \tag{1}$$

Here, g is the interaction strength, $\hat{A}$ is the observable of the system, and $\hat{p}$ is the canonical momentum of the pointer. The weak value in weak measurement is defined as [34]

$$A_w = \frac{\langle \psi_f | \hat{A} | \psi_i \rangle}{\langle \psi_f | \psi_i \rangle}, \tag{2}$$

where $|\psi_i\rangle$ and $|\psi_f\rangle$ are the preselected and postselected states, respectively.

AWVs in weak measurements [23,28] can be defined using the real part or imaginary part of the weak values, described as follows.

(1) Real part of the AWVs: If the real part of the weak value is less than the minimum eigenvalue or greater than the maximum eigenvalue of $\hat{A}$, we call A_w an AWV [23]. Assume $\hat{A}$ can be expressed as $\hat{A} = \sum_a a\Pi^{(a)}$ using the spectral decomposition technique, where a is the eigenvalue and $\Pi^{(a)}$ is the corresponding projector. Because the real part of A_w can be expressed as

$$\text{Re}(A_w) = \sum_a a\text{Re}\left(\frac{\langle \psi_f | \Pi^{(a)} | \psi_i \rangle}{\langle \psi_f | \psi_i \rangle} \right) = \sum_a a\text{Re}\big(\Pi_w^{(a)}\big), \tag{3}$$

a weak value A_w with anomalous real part implies that one of its eigenprojectors satisfies $\text{Re}(\Pi_w^{(a)}) < 0$ [23].

(2) Imaginary part of the AWVs: If the imaginary part of the weak value is not zero, i.e.,

$$\text{Im}(A_w) \neq 0, \tag{4}$$

we also call A_w an AWV. A weak value A_w with anomalous imaginary part also implies that one of its eigenprojectors satisfies $\text{Im}(\Pi_w^{(a)}) < 0$ [28].

B. Noncontextual ontological models

In an operational theory, the primitive elements are preparation and measurement procedures. The theory simply provides rules for calculating the probability $p(k|P, M)$, representing the probability of obtaining an outcome k of measurement M given a preparation P. As an example, suppose we prepare a quantum system in a state $|\psi\rangle$, after

that a positive operator-valued measurement (POVM) $\{E_k\}$ is performed, then quantum theory gives the probability $p(k|P, M) = \langle \psi | E_k | \psi \rangle$.

For an ontological model of an operational theory, the preparation procedure P is represented by a probability distribution $p(\lambda|P)$ over a set of ontic states $\{\lambda \in \Lambda\}$, and the measurement procedure M is represented by a conditional probability $p(k|\lambda, M)$, representing that implementation of M on a state described by λ yields outcome k with probability $p(k|\lambda, M)$. Then, the ontological model gives the prediction $p(k|P, M) = \int d\lambda\, p(k|\lambda, M)p(\lambda|P)$.

Assumptions of noncontextuality are procedural constraints on the ontological model. NCOMs are ontological models which satisfy that if two experimental procedures (preparations or measurements) are operationally equivalent, i.e., giving rise to the same statistics of prediction, then they have an equal representation in the ontological model; in other words, the characterization of each experimental procedure only depends on its equivalence class and does not depend on its context [18].

C. AWVs and contextuality

The authors of Refs. [23,28] proposed and proved a connection between AWVs and the generalized contextuality under certain conditions, and the following theorem was given.

Theorem 1. In an operational interpretation of a physical theory, suppose there is a preparation procedure P_{ψ_i}, a two-outcome sharp measurement procedure M_{ψ_f} that outputs S and F (corresponding to the successful and failed postselection of the state $|\psi_f\rangle$, respectively), and a generalized measurement procedure $\{M_W\}_{z\in R}$, which satisfy the following four conditions.

(1) The preselected state $|\psi_i\rangle$ and the postselected state $|\psi_f\rangle$ are nonorthogonal

$$p_{\psi_f} := p(S|P_{\psi_i}, M_{\psi_f}) = |\langle \psi_f | \psi_i \rangle|^2 > 0. \tag{5}$$

(2) There exists a two-outcome measurement M_ϵ and a probability distribution $p(z)$ with median $z = 0$. Removing the postselection procedure M_{ψ_f}, the weak measurement is equivalent to a two-outcome measurement. That is, for all $z \in R$,

$$p(z \mid P_{\psi_i}, M_W) \simeq p(z-g)p(1 \mid M_\epsilon) + p(z)p(0 \mid M_\epsilon), \tag{6}$$

where g is a positive real number.

(3) There exists a "probability of disturbance" $p_d \in [0, 1]$ (the effect of weak measurements on subsequent measurements) such that, ignoring the outcome of M_W, it affects the postselection in the same way as mixing it with another measurement

$$p(S \mid P_{\psi_i}, M_W, M_{\psi_f}) = (1 - p_d)p(S \mid P_{\psi_i}, M_{\psi_f}) + p_d p(S \mid P_{\psi_i}, M_d), \tag{7}$$

where M_d denotes some other measurement procedure with two outcomes.

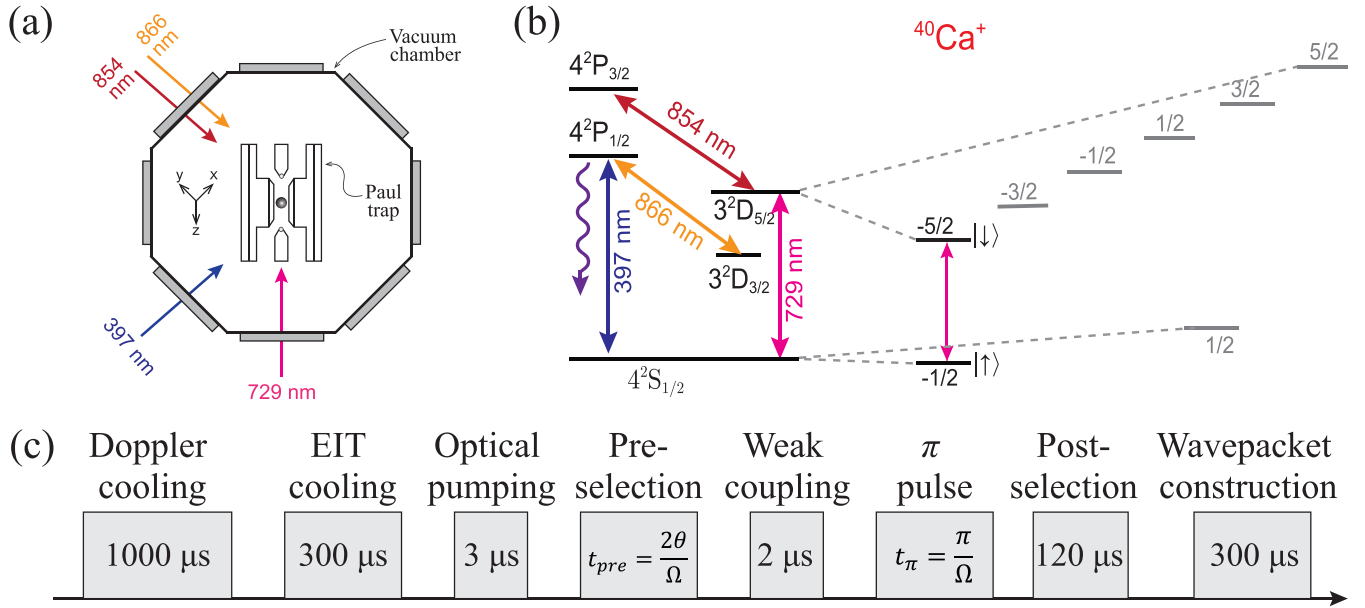(4) The values of z have a negative bias probability of "outweighing" p_d after the successful postselection. That

FIG. 1. (a) Experimental setup. A single ^{40}Ca$^+$ is trapped in a linear Paul trap, which is located in a vacuum chamber. The lasers for quantum manipulation enter the trap by passing through the glass windows of the chamber. (b) The internal electronic states and coupling lasers used. (c) The experimental procedure for the weak measurement using our single trapped ion.

is, by defining $p_{-z} := (p_{\psi_f})^{-1} \int_{-\infty}^{0} p(z, S \mid P_{\psi_i}, M_W, M_{\psi_f}) \mathrm{d}z$, the following two inequalities hold. For the real parts of AWVs,

$$p_{-z} \approx \frac{1}{2} - \frac{1}{\sqrt{\pi}\Delta_z} \mathrm{Re}(\Pi_w) > \frac{1}{2} + \frac{(1 - p_{\psi_f})p_d}{p_{\psi_f}}, \quad (8)$$

where Δ_z is the wavepacket size of the measuring pointer. For the imaginary parts of AWVs

$$p_{-z} \approx \frac{1}{2} - \frac{1}{\sqrt{\pi}\Delta_z} \mathrm{Im}(\Pi_w) > \frac{1}{2} + \frac{(1 - p_{\psi_f})p_d}{p_{\psi_f}}. \quad (9)$$

The authors of Refs. [23,28] proved that there is no noncontextual ontological model for the preparation P_{ψ_i}, measurement $\{M_W\}_{z \in R}$, and postselection of $|\psi_f\rangle$ satisfying the outcome determinism for sharp measurements.

In our experiment of the weak measurement in a single trapped ion, under a set of procedural constraints described by the above conditions (1) to (3), the inequalities $L_R = -\frac{(1-p_{\psi_f})p_d}{p_{\psi_f}} - \frac{1}{\sqrt{\pi}\Delta_z} \mathrm{Re}(\Pi_w) > 0$ and $L_I = -\frac{(1-p_{\psi_f})p_d}{p_{\psi_f}} - \frac{1}{\sqrt{\pi}\Delta_z} \mathrm{Im}(\Pi_w) > 0$ are experimentally verified. Therefore, the violation of NCOMs can be obtained using these results and the connection between AWVs and the generalized contextuality can be established.

III. EXPERIMENTAL IMPLEMENTATION AND RESULT ANALYSIS

A. Experimental setup and procedure

The experimental setup and the main sequence of our experiment are shown in Fig. 1. A single ^{40}Ca$^+$ is produced by the photoionization process and trapped in a blade-shaped linear Paul trap, which is mounted in a vacuum chamber [Fig. 1(a)]. The axial and radial trapping frequencies are $\omega_z =$

$2\pi \times 1.33$ MHz and $\omega_r = 2\pi \times 1.6$ MHz, respectively. Several lasers with different wavelengths enter the trap by passing through the glass windows of the chamber and illuminate on the ion for the quantum manipulation and measurement operations.

The Zeeman sublevels $4S_{1/2}(m_J = -1/2)$ and $3D_{5/2}(m_J = -5/2)$ are used as the spinor states $|\uparrow\rangle$ and $|\downarrow\rangle$, respectively, and their energy level spacing is denoted as $\hbar\omega_0$ [Fig. 1(b)]. A narrow linewidth laser of 729 nm is used to drive the optical quadrupole transition between $|\uparrow\rangle$ and $|\downarrow\rangle$. The 729-nm laser beam enters the trap by passing through two hollow end-cap electrodes, parallel to the axial z direction, resulting in a Lamb-Dicke parameter of $\eta \approx 0.08$. The 397-nm laser, coupling the $S_{1/2}$ state to the short-lived state $P_{1/2}$, is used for Doppler cooling, electromagnetically induced transparency (EIT) cooling and fluorescence detection. The 854-nm and 866-nm lasers are used for pumping the ion out of the D states.

Figure 1(c) shows the whole experimental procedure for the weak measurement using a single trapped ion. The motional ground state of the ion can be prepared by implementing the Doppler cooling for 1000 μs and EIT cooling for 300 μs. Using optical pumping pulse for 3 μs, the internal electronic state of the ion can be initialized to $S_{1/2}(m_J = -1/2)$. The preselected state can be prepared by driving the $|\uparrow\rangle \rightarrow |\downarrow\rangle$ transition for a time $t_{\mathrm{pre}} = 2\theta/\Omega$, where 2θ is the rotation angle and Ω is the coupling Rabi frequency. The weak coupling between the motional state and the spinor state is achieved by a bichromatic light pulse (with the frequencies $\omega_0 \pm \omega_z$) of 2 μs. The postselection by a 397-nm laser pulse of 120 μs retains the data that the electronic state of the ion is $|\downarrow\rangle$. A π pulse of $|\uparrow\rangle \rightarrow |\downarrow\rangle$ transition is needed if the postselected state is $|\uparrow\rangle$. Furthermore, with the photon fluorescence detection method, we can construct the postselected motional wavepacket and obtain the average spatial displacement of the axial motion [30,35–37].

B. Preparation of the preselected state

In our weak measurement scheme, the axial vibrational motion of the ion along the z direction and the spinor states are used as the measuring pointer and measured system, respectively. After Doppler cooling and EIT cooling in sequence, the ion is cooled to the ground state. The obtained axial motional ground state can be described as

$$|\varphi_i(z)\rangle = \left(\frac{1}{2\pi\Delta_z{}^2}\right)^{\frac{1}{4}} e^{-\frac{z^2}{4\Delta_z{}^2}}, \tag{10}$$

where $\Delta_z = \sqrt{\frac{\hbar}{2m\omega_z}} = 9.726$ nm is the width of the ground-state wavepacket and m is the ion's mass. However, the internal state of the ion is initialized to $|\uparrow\rangle$ by optical pumping using 397-nm, 854-nm, and 866-nm lasers. Then we rotate the internal state along the Y axis of the Bloch's sphere by $2\theta = 0.94\pi$ to obtain the preselected state $|\psi_i\rangle = \cos(\theta)|\uparrow\rangle + \sin(\theta)|\downarrow\rangle$.

C. Coupling of measured system and measuring pointer

In the trapped-ion system, the weak coupling of the system and the pointer is achieved by a bichromatic light resonant with the red and blue sidebands at the same time, which is realized via sending the 729-nm laser through an acoustooptic modulator (AOM) driven by two RF signals; the light frequencies are $\omega_0 - \omega_z$ and $\omega_0 + \omega_z$, respectively. Here, we choose the Pauli-x operator $\hat{\sigma}_x$ of the qubit as the system observable. In the Lamb-Dicke approximation, the resulting Hamiltonian of the weak coupling system reads

$$H_I = \frac{\hbar\eta\Omega}{2}(\hat{\sigma}_x \sin\phi_+ - \hat{\sigma}_y \cos\phi_+)[(\hat{a} + \hat{a}^\dagger)\cos\phi_-$$
$$+ i(\hat{a}^\dagger - \hat{a})\sin\phi_-]. \tag{11}$$

The Rabi frequency Ω can be adjusted by changing the intensity of the two RF signals driving the AOM, and here we set it as $\Omega = 2\pi \times 8.24$ KHz. $\hat{a}$ and $\hat{a}^\dagger$ are the annihilation and creation operators for the degree of motional freedom, $2\phi_+ = \phi_{\text{blue}} + \phi_{\text{red}}$ and $2\phi_- = \phi_{\text{blue}} - \phi_{\text{red}}$ represent the sum and difference between the red-sideband laser phase ϕ_{red} and the blue-sideband laser phase ϕ_{blue}. In the experiment, we choose $\phi_+ = \phi_- = \pi/2$, then the interaction Hamiltonian can be written as

$$H_I = \frac{i\hbar(\hat{a}^\dagger - \hat{a})}{2}\eta\Omega\hat{\sigma}_x = \eta\Omega\Delta_z\hat{\sigma}_x\hat{p}, \tag{12}$$

where the canonical momentum $\hat{p} = \frac{i\hbar(\hat{a}^\dagger - \hat{a})}{2\Delta_z}$. By performing the bichromatic light with a duration $t = 2\,\mu s$, we obtain a coupling strength $g = \eta\Omega t = 0.01$ between the system and the pointer and implement a spin-dependent displacement. In this case, the probability of disturbance $p_d = 1 - \exp[-g^2/4] = 0.00236$ is small enough [27] and meets the requirement of Eq. (7) [28].

D. Postselection

The initial state for the internal and motional degrees of the ion is $|\psi\rangle = |\psi_i\rangle \otimes |\varphi_i(z)\rangle$. After the weak coupling, by driving the ion to its fast decaying energy level $4P_{1/2}$ (with a lifetime of about 7.1 ns) with 397-nm laser, we can distinguish

between the states $|\uparrow\rangle$ and $|\downarrow\rangle$. For our trapped ion system, only the state $|\downarrow\rangle$ can be postselected directly without destroying the motional wavepacket as no photons are scattered. However, the other states can be indirectly postselected with the help of appropriate one-qubit rotations. In our experiment, we take the result of postselected state $|\uparrow\rangle$ to verify the noncontextuality inequality. In this case, the preselected state and the postselected state satisfy Eq. (5). To postselect $|\uparrow\rangle$, a 729-nm π-pulse resonant with the $|\uparrow\rangle \rightarrow |\downarrow\rangle$ transition is implemented before the photon fluorescence detection. After postselection, the wave function for the external motion is (choosing Δ_z as the unit of $\hat{z}$):

$$|\varphi_f(z)\rangle = \frac{\sin\left(\theta + \frac{\pi}{4}\right)e^{-\frac{(z-g)^2}{4}} + \cos\left(\theta + \frac{\pi}{4}\right)e^{-\frac{(z+g)^2}{4}}}{\sqrt[4]{2\pi}\sqrt{1 + \cos(2\theta)e^{-\frac{g^2}{2}}}}. \tag{13}$$

Because the probability of successful postselection is 0.89%, only about 222 experiments are effective for a total of about 25 000 experimental cycles. After completing the wavepacket reconstruction, we fit the reconstructed data of the wavepacket and obtain that, the displacement of the center position of the motional wavepacket is about 0.108 ± 0.01173 (in units
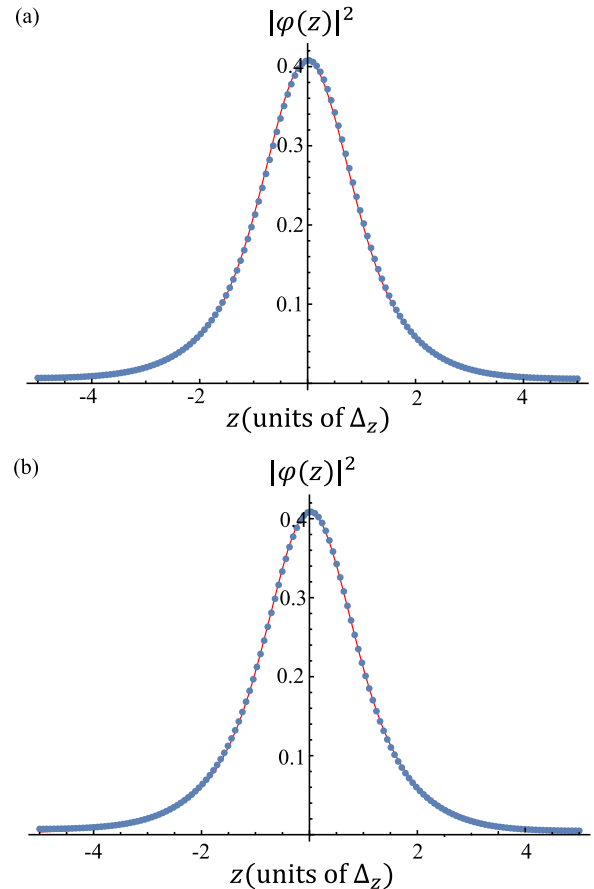

FIG. 2. Wavepackets of the ground state (a) before and (b) after the data acquisition process of our weak measurement experiment. The red solid lines represent the theoretical results. The blue data points represent the ground-state wavepackets reconstructed according to the experimental data, and their central positions are 0.009 ± 0.001 and 0.009 ± 0.0013, respectively. It can be seen that the center positions have very small deviations from the theoretical values.
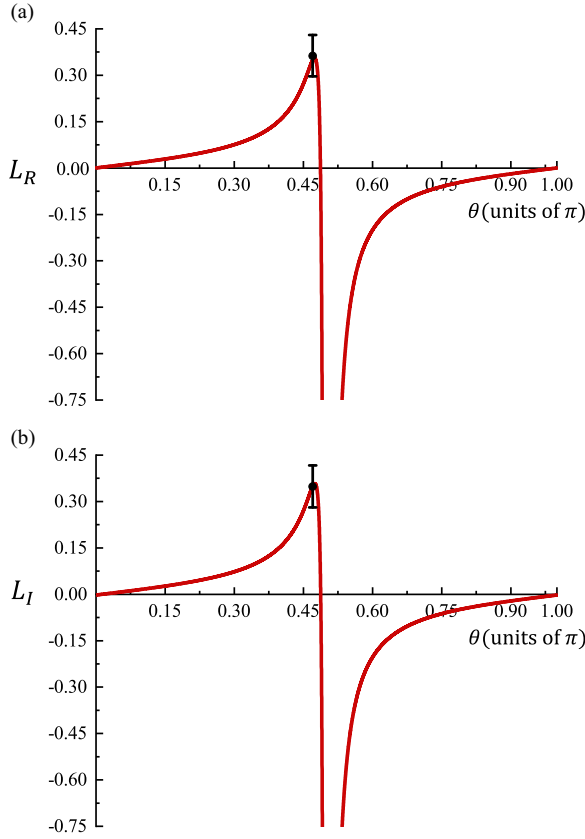
FIG. 3. The solid red lines are plots of (a) L_R and (b) L_I, respectively, and the variable is the phase angle θ of the preselected state. The black dots are the experimental results ($L_R^{\exp} = 0.3605 \pm 0.0674$, $L_I^{\exp} = 0.3489 \pm 0.0679$) with the preselected state $\cos(\theta)|\uparrow\rangle + \sin(\theta)|\downarrow\rangle$, the postselected state $|\uparrow\rangle$, $\theta = 0.47\pi$, and $g = 0.01$. The experimental results obviously violate the NCOMs.
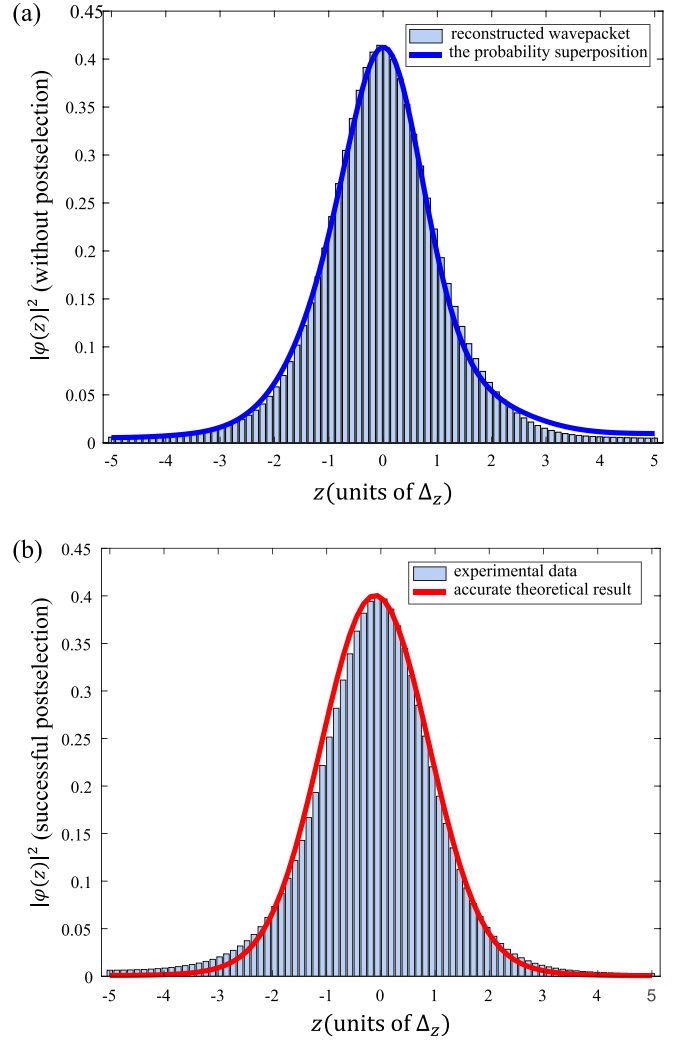

FIG. 4. (a) The histogram represents the wavepacket reconstructed directly without postselection after the internal states and external motional states are weakly coupled. The blue line shows the superimposed wavepackets with postselected state $|\uparrow\rangle$ and $|\downarrow\rangle$ in the weak measurement experiment. It can be seen that the two wavepackets (the histogram and the blue line) are in good agreement, which indicates that our experiment meets the requirement in Eq. (6) that weak measurement is equivalent to a two-outcome measurement. (b) The histogram represents the wavepacket reconstructed with the successful postselection of $|\uparrow\rangle$, which agrees well with the theoretical curve.

of Δ_z). And the displacement of the axial motion is $\delta_z = g \sin(2\theta)/[\exp(-g^2/2)\cos(2\theta) + 1] \approx 0.1055$ in theory.

Similarly, for the cases where the weak value is imaginary, we choose the preselected state $\cos(\theta)|\uparrow\rangle + \sin(\theta)|\downarrow\rangle$, and reconstruct the wavepacket with the postselected state $|\uparrow\rangle$. Different from the real part of the weak value, the observable of the system is selected as the Pauli-y operator $\hat{\sigma}_y$ of the qubit, and the bichromatic light phases $\phi_+ = \pi$ and $\phi_- = \pi/2$ are used in the displacement operation. Then, by using the definition of weak value in Eq. (2), A_w can be derived to be pure imaginary numbers. For imaginary weak values, according to the authors of Ref. [38], the wavepacket displacement after postselection can be observed in the same direction as defined using the pointer operator in Eq. (11), which is $\hat{p}$ when choosing $\phi_- = \pi/2$. When the postselected state is $|\uparrow\rangle$, the wavepacket displacement is $\delta_p = 0.106 \pm 0.0117$ (in units of $\Delta_p = \frac{\hbar}{2\Delta_z}$). The displacement of the axial motion is $\delta_p = g \sin(2\theta)/[\exp(-g^2/2) + \cos(2\theta)] \approx 0.1061$ in theory.

It can be seen that, in our weak measurement experiment of the trapped ion, the interaction strength selected is only 0.01, and the postselection probability is only 0.89%. A large amount of data need to be collected, and the experimental duration is very long, so the stability of the experimental system is particularly important. To monitor the stability of

the experimental system and increase the confidence level of the experimental data, we directly reconstruct the same ground-state wavepacket of the pointer state before and after the data acquisition process of our weak measurement experiment, respectively. As shown in Fig. 2, the center positions of the ground-state wavepackets are 0.009 ± 0.001 and 0.009 ± 0.0013, respectively, and the measurement errors are within the acceptable range, indicating that our experimental system is relatively stable during the experiment.

E. AWVs and contextuality

As shown in Fig. 3, the AWVs of real and imaginary parts by experiments are in good agreement with Eqs. (8)

and (9). According to the above measurement results, we obtain $L_R^{\text{exp}} = 0.3605 \pm 0.0674$ and $L_I^{\text{exp}} = 0.3489 \pm 0.0679$.

Verification of Theorem 1

To verify the validity of our experimental results, we need to prove that the conditions in Theorem 1 are fulfilled. Note that we already verified Eqs. (5) and (7), so only the validity of Eq. (6) remains to be verified. After completing the weak coupling procedure, a 854-nm laser pulse with a duration of 120 μs is used to pump the population from $|\downarrow\rangle$ to $|\uparrow\rangle$, and then we directly reconstruct the pointer state wavepacket without postselection. As shown in Fig. 4(a), we perform the probability superposition on wavepackets with postselected states $|\uparrow\rangle$ and $|\downarrow\rangle$, and find that the pointer state wavepacket without postselection agrees well with this superimposed wavepacket. In Fig. 4(b), the experimentally obtained pointer wavepacket with the successful postselection of the state $|\uparrow\rangle$ is also given, which agrees well with the theoretical result.

Now that all the conditions in Theorem 1 have been verified, we can evaluate that our experimental results clearly violate the noncontextual bounds of the quantities in inequalities Eqs. (8) and (9). The connection between the real and imaginary parts of AWVs and the generalized contextuality is demonstrated simultaneously.

IV. CONCLUSION

We use a single trapped $^{40}\text{Ca}^+$ ion to perform weak measurement experiments of purely atomic degrees of freedom and demonstrate the connection between both the real and imaginary parts of AWVs and the generalized contextuality. In the experiment, the measurement error of the ground-state wavepacket is within the acceptable range, indicating that our experimental system is stable during the experiment. To ensure that the weak measurement experiment meets the verification conditions, we select the appropriate pre and postselected states. The experiment is carried out when the coupling strength is only 0.01, and the postselection probability is only 0.89% to ensure that the weak measurement process has little influence on the subsequent measurement. In addition, the pointer-state wavepackets of successful postselection, failed postselection, and no postselection measurement are used to verify the two-outcome measurement equivalence of weak measurement. The good scalability, stability, and flexible controllability of our trapped ion system enable us to complete the measurement of the real and imaginary parts of AWVs. Our results are important for understanding the role of contextuality in quantum mechanics, as well as for understanding the particular properties of AWVs.

[1] C. Budroni, A. Cabello, O. Gühne, M. Kleinmann, and J. Å. Larsson, Rev. Mod. Phys. **94**, 045007 (2022).

[2] S. Kochen and E. P. Specker, J. Math. Mech. **17**, 59 (1967).

[3] A. Peres, J. Phys. A: Math. Gen. **24**, L175 (1991).

[4] A. Peres and M. E. Mayer, Phys. Today **47**(12), 65 (1994).

[5] M. Kernaghan, J. Phys. A: Math. Gen. **27**, L829 (1994).

[6] A. Cabello, J. Estebaranz, and G. García-Alcaine, Phys. Lett. A **212**, 183 (1996).

[7] R. Clifton, Am. J. Phys. **61**, 443 (1993).

[8] A. A. Klyachko, M. A. Can, S. Binicioğlu, and A. S. Shumovsky, Phys. Rev. Lett. **101**, 020403 (2008).

[9] S. Yu and C. H. Oh, Phys. Rev. Lett. **108**, 030402 (2012).

[10] X. Zhang, M. Um, J. Zhang, S. An, Y. Wang, D. L. Deng, C. Shen, L.-M. Duan, and K. Kim, Phys. Rev. Lett. **110**, 070401 (2013).

[11] F. M. Leupold, M. Malinowski, C. Zhang, V. Negnevitsky, A. Cabello, J. Alonso, and J. P. Home, Phys. Rev. Lett. **120**, 180401 (2018).

[12] P. Wang, J. Zhang, C.-Y. Luan, M. Um, Y. Wang, M. Qiao, T. Xie, J.-N. Zhang, A. Cabello, and K. Kim, Sci. Adv. **8**, eabk1660 (2022).

[13] M. Michler, H. Weinfurter, and M. Żukowski, Phys. Rev. Lett. **84**, 5457 (2000).

[14] B. Marques, J. Ahrens, M. Nawareg, A. Cabello, and M. Bourennane, Phys. Rev. Lett. **113**, 250403 (2014).

[15] O. Moussa, C. A. Ryan, D. G. Cory, and R. Laflamme, Phys. Rev. Lett. **104**, 160501 (2010).

[16] S. B. van Dam, J. Cramer, T. H. Taminiau, and R. Hanson, Phys. Rev. Lett. **123**, 050401 (2019).

[17] M. Jerger, Y. Reshitnyk, M. Oppliger, A. Potočnik, M. Mondal, A. Wallraff, K. Goodenough, S. Wehner, K. Juliusson, N. K. Langford, and A. Fedorov, Nat. Commun. **7**, 12930 (2016).

[18] R. W. Spekkens, Phys. Rev. A **71**, 052108 (2005).

[19] D. Schmid, H. Du, J. H. Selby, and M. F. Pusey, Phys. Rev. Lett. **129**, 120403 (2022).

[20] D. Schmid and R. W. Spekkens, Phys. Rev. X **8**, 011015 (2018).

[21] M. Lostaglio and G. Senno, Quantum **4**, 258 (2020).

[22] R. W. Spekkens, D. H. Buzacott, A. J. Keehn, B. Toner, and G. J. Pryde, Phys. Rev. Lett. **102**, 010401 (2009).

[23] M. F. Pusey, Phys. Rev. Lett. **113**, 200401 (2014).

[24] J. Dressel, M. Malik, F. M. Miatto, A. N. Jordan, and R. W. Boyd, Rev. Mod. Phys. **86**, 307 (2014).

[25] G. C. Knee, J. Combes, C. Ferrie, and E. M. Gauger, Quantum Meas. Quantum Metrol. **3**, 1 (2016).

[26] J. Tollaksen, J. Phys. A: Math. Theor. **40**, 9033 (2007).

[27] F. Piacentini, A. Avella, M. P. Levi, R. Lussana, F. Villa, A. Tosi, F. Zappa, M. Gramegna, G. Brida, I. P. Degiovanni, and M. Genovese, Phys. Rev. Lett. **116**, 180401 (2016).

[28] R. Kunjwal, M. Lostaglio, and M. F. Pusey, Phys. Rev. A **100**, 042116 (2019).

[29] C.-W. Wu, J. Zhang, Y. Xie, B.-Q. Ou, T. Chen, W. Wu, and P.-X. Chen, Phys. Rev. A **100**, 062111 (2019).

[30] Y. Pan, J. Zhang, E. Cohen, C.-w. Wu, P.-X. Chen, and N. Davidson, Nat. Phys. **16**, 1206 (2020).

[31] G. Araneda, S. Walser, Y. Colombe, D. B. Higginbottom, J. Volz, R. Blatt, and A. Rauschenbeutel, Nat. Phys. **15**, 17 (2019).

[32] T. Denkmayr, H. Geppert, H. Lemmel, M. Waegell, J. Dressel, Y. Hasegawa, and S. Sponar, Phys. Rev. Lett. **118**, 010402 (2017).

[33] J. P. Groen, D. Ristè, L. Tornberg, J. Cramer, P. C. de Groot, T. Picot, G. Johansson, and L. DiCarlo, Phys. Rev. Lett. **111**, 090506 (2013).

[34] Y. Aharonov, D. Z. Albert, and L. Vaidman, Phys. Rev. Lett. **60**, 1351 (1988).

[35] S. Wallentowitz and W. Vogel, Phys. Rev. Lett. **75**, 2932 (1995).

[36] F. Zähringer, G. Kirchmair, R. Gerritsma, E. Solano, R. Blatt, and C. F. Roos, Phys. Rev. Lett. **104**, 100503 (2010).

[37] J. Zhang, C.-W. Wu, Y. Xie, W. Wu, and P.-X. Chen, Chin. Phys. B **30**, 033201 (2021).

[38] R. Jozsa, Phys. Rev. A **76**, 044103 (2007).